High-spin intrinsic and rotational states in the stable nucleus ^{177}Hf: Evidence for reaction-dependent spin population

S. M. Mullins, A. P. Byrne,* G. D. Dracoulis, T. R. McGoram, and W. A. Seale†
Department of Nuclear Physics, RSPhysSE, The Australian National University, Canberra, ACT 0200, Australia
(Received 20 April 1998)

The stable nucleus ^{177}Hf was studied with time-correlated particle-γ-γ techniques following the reaction ^{176}Yb(^{9}Be,$\alpha 4n$)^{177}Hf at a beam energy of 70 MeV. New high-spin states include extensions to three-quasiparticle bands based on the $K^{\pi}=23/2^{+}$ and $25/2^{-}$ configurations, together with a new band associated with the $K^{\pi}=19/2^{-}$, $T_{1/2}=56$ μs isomer. Moreover, the band based on the five-quasiparticle $T_{1/2}=51$ minute, $K^{\pi}=37/2^{-}$ state has been found, and a band assigned to a new $K^{\pi}=39/2^{+}$, five-quasiparticle state. Values of $(g_K-g_R)/Q_0$ agree well with the configuration assignments made to new and previously known bands. Comparison with multiquasiparticle calculations that incorporate a Lipkin-Nogami treatment of pairing correlations with blocking, suggests that all of the most favored three- and five-quasiparticle states have been observed. The dependence of the γ-ray intensities on the angular yields of the α particles suggests that the population arises from two entry distributions: one associated with complete fusion of the beam with the target, the other with incomplete fusion. [S0556-2813(98)06408-5]

PACS number(s): 27.70.+q, 23.20.Lv, 21.10.Re

I. INTRODUCTION

The stable nucleus ^{177}Hf is located in the region of deformation near $A=180$. In this region, collective rotational behavior coexists with intrinsic quasiparticle modes of excitation as a means with which to form the yrast line. The quasiparticle excitations arise from the coupling of a few orbitals that have a large angular-momentum projection, Ω, on the nuclear symmetry axis. The projection of the total nuclear angular momentum onto the symmetry axis is, to a good approximation, a constant of motion so that the associated quantum number K $(=\Sigma_i\Omega_i)$ is nearly conserved. Transitions of multipolarity λ between states where $\Delta K>\lambda$, are in principle strictly forbidden, but in practice hindered so that many excited multiquasiparticle states are metastable (isomeric) in character.

Two of the longest-lived K isomers known are found in ^{177}Hf; one is the $K^{\pi}=23/2^{+}$ three-quasiparticle state which has $T_{1/2}=1.1$ s [1,2], the other is the $K^{\pi}=37/2^{-}$ five-quasiparticle state which has $T_{1/2}=51$ min [3]. Previous studies were able to associate a rotational band with former, but not with the latter. Since such bands are an important means with which to characterize the multiquasiparticle configuration of the K isomer, one aim of the present study was to identify the band associated with the $K^{\pi}=37/2^{-}$ state. The only available conventional fusion/neutron-evaporation reaction is ^{176}Yb(α,$3n$)^{177}Hf, in which the input angular momentum is too low to populate strongly states above the $K^{\pi}=37/2^{-}$ isomer. This necessitated the use of the ^{176}Yb(^{9}Be,$\alpha 4n$)^{177}Hf reaction which should have a higher input angular momentum. A similar approach led to the observation of the band based on the $T_{1/2}=31$ year, $K^{\pi}=16^{+}$ isomer in ^{178}Hf [4].

II. EXPERIMENT

The measurement was performed with the CAESAR spectrometer [5] in conjunction with a compact array of charged-particle detectors [6]. The former consists of six hyperpure n-type germanium detectors, while the latter is constituted by 14 fast-slow plastic scintillators in which charged-particle detection and identification is performed via the Phoswich technique. This arrangement was used to collect time-correlated particle-γ-γ coincidences when a 4.6 mg/cm^2 ^{176}Yb target-foil (enriched to 96%) was bombarded with ^{9}Be ions, which were supplied at an energy of 70 MeV by the ANU 14UD Pelletron accelerator. Particle-γ data were also taken. The front particle-detectors were shielded from scattered beam particles with Al absorber foils of 65 mg/cm^2 thickness. All events within 856 ns of a detected particle were recorded. States in ^{177}Hf were populated via the $\alpha 4n$ exit channel, where the α-particle yield arises from two processes. One is conventional fusion evaporation from a ^{185}W* compound system produced by complete fusion of the beam with the target. The other is from breakup of the ^{9}Be in the entrance channel into $\alpha+\alpha+n$. One of the α particles can then fuse with the target, perhaps with simultaneous capture of the neutron, while the other α particle continues with a velocity essentially equal to that of the beam. This process is known as ''incomplete fusion'' or ''massive transfer'' [7–9]. In the present case, the mechanism can be viewed approximately as beam-breakup with subsequent fusion and evaporation of the form ^{176}Yb(''^{5}He,''$4n$)^{177}Hf.

A ^{152}Eu source was placed at the target position to enable energy and efficiency calibration of the HPGe detectors. It was not possible to obtain a precise calibration of the

*Joint appointment with the Department of Physics, The Faculties, The Australian National University, Canberra, ACT 0200, Australia.
†Permanent address: Laboratório Pelletron, Departamento de Física Nuclear, Instituto de Física, Universidade de São Paulo, São Paulo, Brazil.

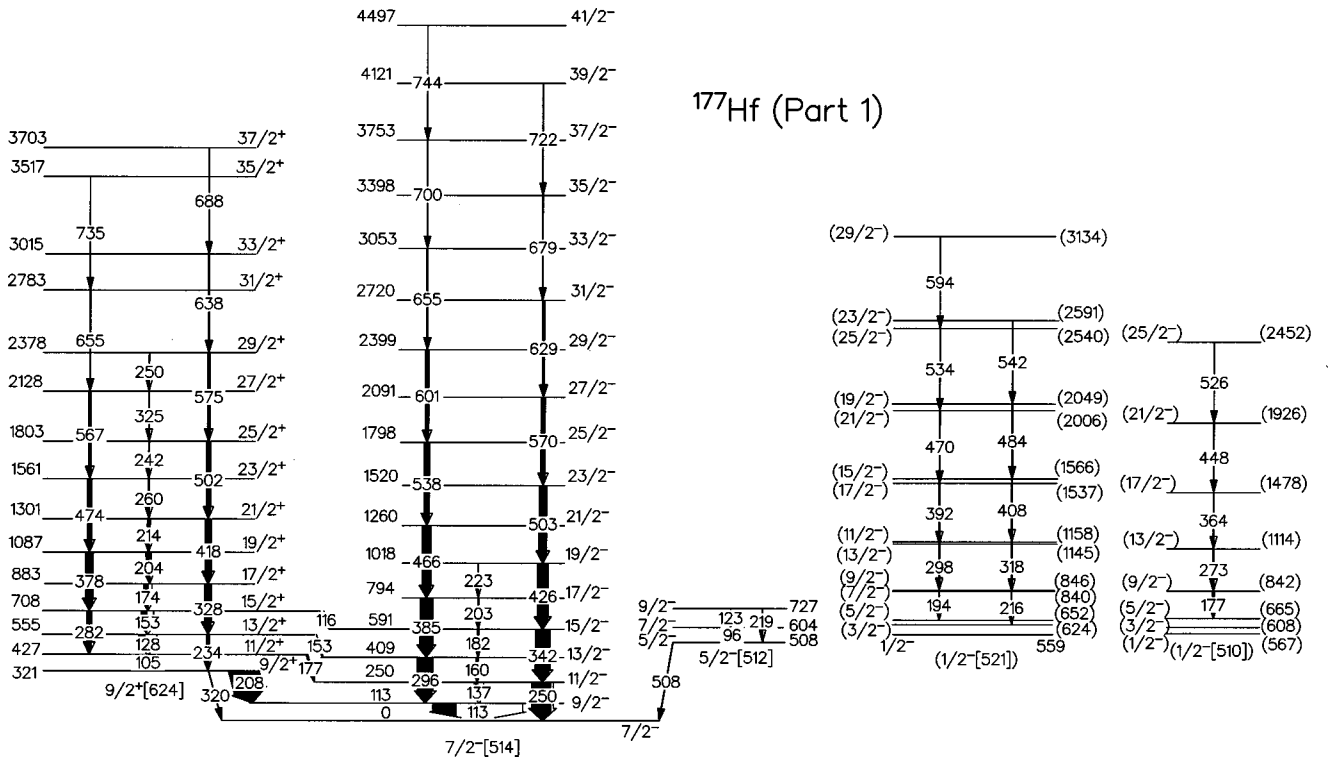

FIG. 1. Partial level scheme for ^{177}Hf in which single quasineutron states and associated rotational bands are shown.

particle-detector ball, since the available sources produced α particles with insufficient energy to penetrate the absorber foils on the front elements. The possibility of extracting an approximate *in situ* efficiency calibration will be discussed in Sec. V C.

III. DATA ANALYSIS AND RESULTS

A. Particle-γ-γ data

1. Construction of the level scheme

The time-correlated particle-γ-γ coincidence data were sorted offline into particle-gated E_γ-E_γ matrices with different time conditions. No new isomeric decays were found in ^{177}Hf within the range of experimental sensitivity ($\sim$10–2500 ns). The main analysis was carried out with two matrices; one required that an α particle was detected in the forward particle detectors, which subtended angles covering $\sim$20° to 60° with respect to the beam axis, while the other required that an α particle was detected at more backward angles, in either the middle (60° to 100°) or backward rings (100° to 140°). In each case a condition of $\pm$140 ns was required for the γ-γ time differences, centered on the ''prompt'' peak of the total time-difference spectrum. The final symmetrized matrices that were generated contained 19.7×10^6 counts (forward-α selected) and 4.3×10^6 counts (middle- or back-α selected). Coincidence intensities for known and new bands were obtained from the two matrices. The level scheme for ^{177}Hf is shown in Figs. 1, 2, and 3. The γ-ray transition energies and intensities are listed in Table I. They were extracted from a two-dimensional fit to the forward-gated matrix with the code ESCL8R [10]. The intensities of the transitions to the ground state and to the long-lived isomers were obtained from intensity balances.

2. Extraction of F/(M-B) intensity ratios

Coincidence intensities were extracted from the forward-gated and middle/back-gated matrices. A ''Forward/Middle-Back'' (F/M-B) γ-γ intensity ratio was generated for each band:

$$R(\text{F/M-B}) = \frac{I_{\gamma\gamma}\,(\text{Forward-gated})}{I_{\gamma\gamma}\,(\text{Middle/Back-gated})}.$$

This provided a guide with which to assign new bands to a particular hafnium isotope that could not otherwise be placed through either prompt or delayed coincidences. The F/(M-B) intensity ratios are shown in Fig. 4 for transitions from ^{178}Hf, ^{177}Hf, and ^{176}Hf. Open data points correspond to previously known transitions, and new transitions that were in coincidence with them. As has been discussed in previous publications [11,4], the isotope that is populated with fewest evaporated neutrons (^{178}Hf in the present case) has the relatively largest yield when a forward-going α particle is detected. This feature can be used as a guide to assign new bands that do not show coincidences with any known transitions. Such transitions are represented by filled data points in Fig. 4.

3. Angular correlations

Transition multipolarities were inferred from the method of directional correlations from oriented (DCO) states. Two matrices were produced for the DCO analysis. One contained γ-γ coincidences that involved only the forward (48°) and backward (145°) HPGe detectors, while the other required a coincidence of a middle (97°) detector with either a forward or backward detector. A DCO ratio of the form

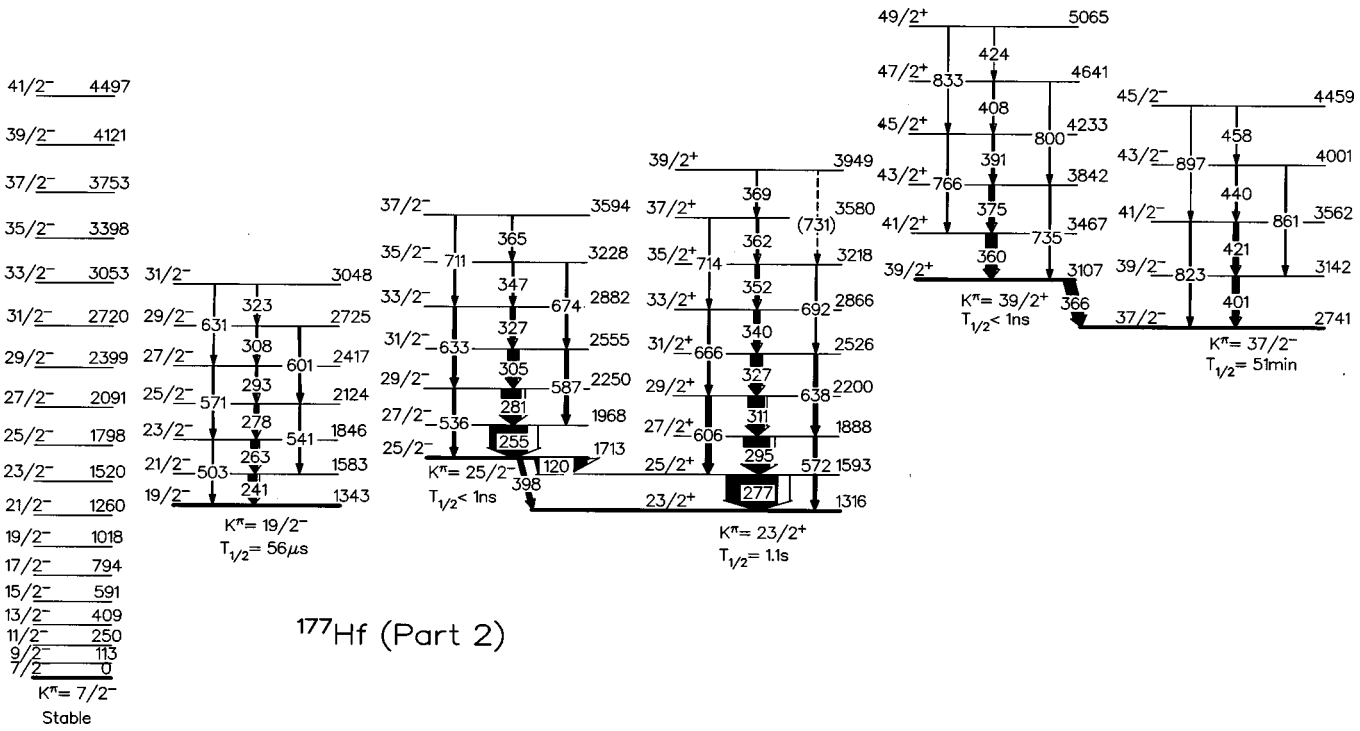

FIG. 2. Partial level scheme for ^{177}Hf in which firmly assigned three- and five-quasineutron states are shown, along with their associated rotational bands. Decays from long-lived states were not observed in the present measurement, and are therefore not shown in the figure. The levels of the ground-state rotational band are also shown to provide an energy scale.

$$R_{DCO}=\frac{I_{\gamma\gamma}(48°+145°)}{I_{\gamma\gamma}(97°)}$$

was obtained, where in each case the gating transition was detected at 48° or 145°. Ideally the gating transition should be of stretched ($\Delta J=2$) quadrupole character, and this was carried out where possible for ^{177}Hf. These values are listed under ''$R_{\Delta J=2}$'' in Table I. In many cases, however, this was not possible, and a stretched $\Delta J=1$ cascade transition had to be used. This introduced a dependence of the DCO ratio on the mixing ratio of gating (and sometimes the measured) transition, but enabled pure and mixed $\Delta J=1$ transitions to be distinguished. These results are listed under ''$R_{\Delta J=1}$'' in Table I.

B. Particle-γ data: Angular distributions

The angular distributions were obtained by summing particle-gated γ-ray spectra for each pair of detectors at the

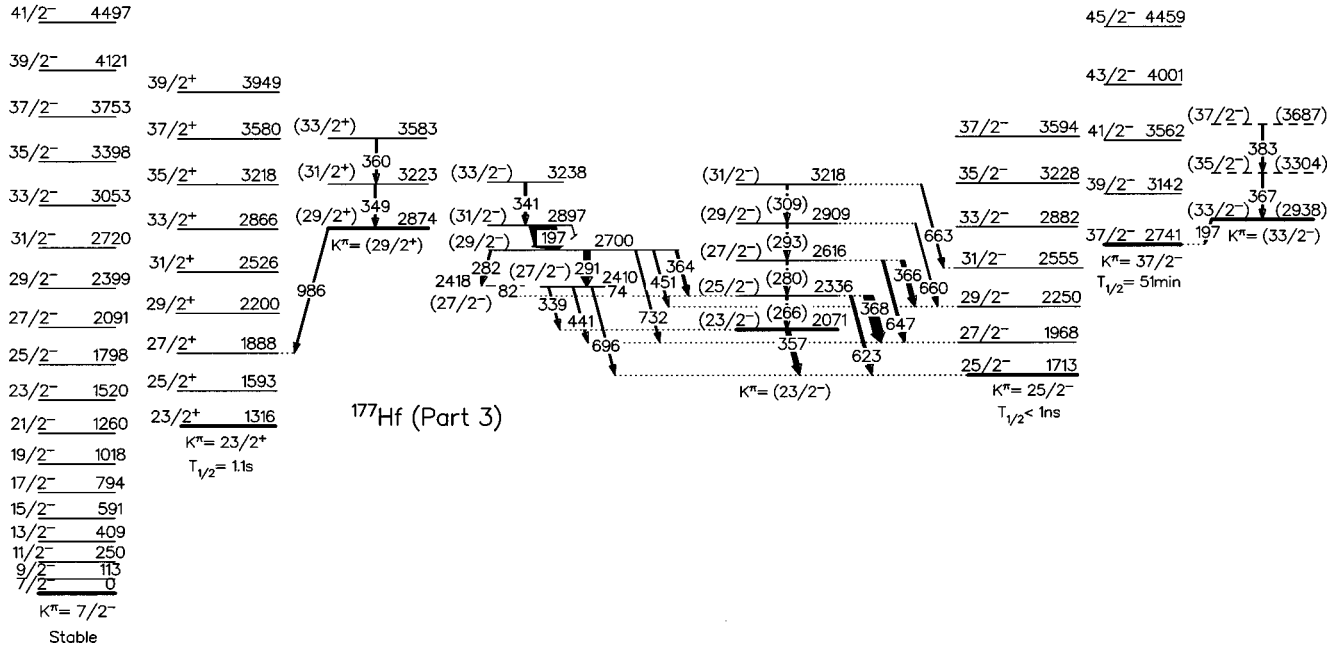

FIG. 3. Partial level scheme for ^{177}Hf in which tentatively identified multiquasiparticle states and associated levels are shown.

TABLE I. Measured and derived quantities for γ-ray transitions in ^{177}Hf. The error on the γ-ray energies is estimated to be ± 0.2 keV.

E_γ(keV)	I_γ	$E_{\rm level}$(keV)	A_2/A_0	$R_{\Delta J=2}$	$R_{\Delta J=1}$	$(J^\pi,K)_i \rightarrow (J^\pi,K)_f$
74.3	3.7(0.4)	2409.8				$(27/2^-,23/2) \rightarrow (25/2^-,23/2)$
82.2	10.7(0.8)	2418.6				$(27/2^-,23/2) \rightarrow (25/2^-,23/2)$
96.4	3.6(1.0)	604.4				$7/2^-,5/2 \rightarrow 5/2^-,5/2$
105.3	105.4(3.7)	426.5	−0.25(2)	0.40(6)	0.40(4)	$11/2^+,9/2 \rightarrow 9/2^+,9/2$
112.9	995.2(24.4)	113.1	−0.13(1)	0.55(7)	0.67(11)	$9/2^-,7/2 \rightarrow 7/2^-,7/2$
116.5	1.9(0.6)	708.2				$15/2^+,9/2 \rightarrow 15/2^-,7/2$
120.4	389.2(12.6)	1713.5	0.31(1)		0.97(3)	$25/2^-,25/2 \rightarrow 25/2^+,23/2$
123.1	2.2(0.8)	727.0				$9/2^-,5/2 \rightarrow 7/2^-,5/2$
128.4	126.0(4.2)	555.0	−0.53(2)	0.63(7)	0.50(5)	$13/2^+,9/2 \rightarrow 11/2^+,9/2$
136.6	77.7(4.7)	249.6	−0.41(2)	0.46(6)	0.81(10)	$11/2^-,7/2 \rightarrow 9/2^-,7/2$
153.1	119.6(4.0)	708.2	−0.52(2)	0.35(10)	0.50(3)	$15/2^+,9/2 \rightarrow 13/2^+,9/2$
153.3	1.5(0.8)	555.0				$13/2^+,9/2 \rightarrow 13/2^-,7/2$
159.6	26.8(1.3)	409.3	−0.12(4)	0.71(9)		$13/2^-,7/2 \rightarrow 11/2^-,7/2$
174.3	94.1(3.2)	882.6	−0.47(3)	0.53(9)	0.46(3)	$17/2^+,9/2 \rightarrow 15/2^+,9/2$
176.5	27.7(1.9)	(665)				$(9/2^+,1/2) \rightarrow (5/2^-,1/2)$
176.9	34.8(1.6)	426.5				$11/2^+,9/2 \rightarrow 11/2^-,7/2$
181.8	16.3(1.0)	591.2		0.51(13)		$15/2^-,7/2 \rightarrow 13/2^-,7/2$
193.6	24.0(1.9)	(840.1)				$(9/2^-,1/2) \rightarrow (5/2^-,1/2)$
196.5	12.9(2.2)	2937.5				$(33/2^-,33/2) \rightarrow 37/2^-,37/2$
196.6	52.8(1.9)	2897.2	−0.28(2)		0.64(6)	$(31/2^-,23/2) \rightarrow (29/2^-,23/2)$
203.0	10.1(0.9)	794.2				$17/2^-,7/2 \rightarrow 15/2^-,7/2$
204.0	68.6(2.4)	1086.6	−0.48(3)	0.54(7)	0.42(4)	$19/2^+,9/2 \rightarrow 17/2^+,9/2$
208.3	608.4(20.7)	321.2	0.26(1)	0.96(12)	1.10(7)	$9/2^+,9/2 \rightarrow 9/2^-,7/2$
214.3	42.9(1.8)	1300.9		0.53(14)	0.34(6)	$21/2^+,9/2 \rightarrow 19/2^+,9/2$
216.1	16.0(1.0)	(846.0)				$(7/2^-,1/2) \rightarrow (3/2^-,1/2)$
218.5	3.3(1.2)	727.0				$9/2^-,5/2 \rightarrow 5/2^-,5/2$
223.3	6.0(7)	1017.5				$19/2^-,7/2 \rightarrow 17/2^-,7/2$
233.8	48.4(2.0)	555.0	0.03(2)	1.16(29)		$13/2^+,9/2 \rightarrow 9/2^+,9/2$
240.6	63.1(3.4)	1582.5				$21/2^-,19/2 \rightarrow 19/2^-,19/2$
249.6	412.4(27.7)	249.6	0.14(1)	0.94(6)		$11/2^-,7/2 \rightarrow 7/2^-,7/2$
254.8	291.2(9.3)	1968.3	0.25(1)		0.95(8)	$27/2^-,25/2 \rightarrow 25/2^-,25/2$
260.0	17.8(1.0)	1560.9		0.46(11)		$23/2^+,9/2 \rightarrow 21/2^+,9/2$
263.0	52.5(2.9)	1846.1				$23/2^-,19/2 \rightarrow 21/2^-,19/2$
272.9	27.7(1.9)	(932.2)				$(13/2^-,1/2) \rightarrow (9/2^-,1/2)$
277.3	637.0(15.0)	1593.0	0.16(1)		0.88(7)	$25/2^+,23/2 \rightarrow 23/2^+,23/2$
278.2	25.8(2.2)	2124.3				$25/2^-,19/2 \rightarrow 23/2^-,19/2$
281.4	152.2(5.0)	2249.6	0.20(4)		0.90(5)	$29/2^-,25/2 \rightarrow 27/2^-,25/2$
281.8	103.2(3.7)	708.2	0.30(2)		1.14(22)	$15/2^+,9/2 \rightarrow 11/2^+,9/2$
282.3	3.9(9)	2700.6				$(29/2^-,23/2) \rightarrow (27/2^-,23/2)$
290.8	42.8(1.8)	2700.6			0.75(13)	$(29/2^-,23/2) \rightarrow (27/2^-,23/2)$
292.6	12.4(1.4)	2416.8				$27/2^-,19/2 \rightarrow 25/2^-,19/2$
295.1	204.1(7.5)	1888.0	0.18(3)		0.77(4)	$27/2^+,23/2 \rightarrow 25/2^+,23/2$
296.5	309.1(12.1)	409.3	0.25(2)	0.95(4)	1.01(9)	$13/2^-,7/2 \rightarrow 9/2^-,7/2$
297.7	24.4(1.9)	1144.7				$(13/2^-,1/2) \rightarrow (9/2^-,1/2)$
305.4	71.9(2.6)	2555.1			0.90(6)	$31/2^-,25/2 \rightarrow 29/2^-,25/2$
308.1	11.9(1.3)	2724.8				$29/2^-,19/2 \rightarrow 27/2^-,19/2$
308.6	1.4(0.7)	3217.8				$(31/2^-,23/2) \rightarrow (29/2^-,23/2)$
311.5	127.8(4.8)	2199.5			0.74(5)	$29/2^+,23/2 \rightarrow 27/2^+,23/2$
317.8	15.6(1.7)	(1157.9)				$(11/2^-,1/2) \rightarrow (7/2^-,1/2)$
321.1	16.2(5.5)	321.2	0.47(7)			$9/2^+,9/2 \rightarrow 7/2-,7/2$
323.2	5.7(1.0)	3047.8				$31/2^-,19/2 \rightarrow 29/2^-,19/2$
326.5	78.6(3.3)	2525.9			0.78(6)	$31/2^+,23/2 \rightarrow 29/2^+,23/2$
327.3	31.3(1.6)	2882.4			0.85(14)	$33/2^-,25/2 \rightarrow 31/2^-,25/2$
327.7	132.9(4.6)	882.6	0.18(2)	0.84(22)	1.26(14)	$17/2^+,9/2 \rightarrow 13/2^+,9/2$
339.4	8.2(9)	2409.8				$(27/2^-,23/2) \rightarrow (23/2^-,23/2)$

TABLE I. (*Continued*).

E_γ(keV)	I_γ	E_{level}(keV)	A_2/A_0	$R_{\Delta J=2}$	$R_{\Delta J=1}$	$(J^\pi,K)_i \rightarrow (J^\pi,K)_f$
340.1	40.4(2.0)	2865.9			0.96(10)	$33/2^+,23/2 \rightarrow 31/2^+,23/2$
340.6	12.3(1.1)	3237.7				$(33/2^-,23/2) \rightarrow (31/2^-,23/2)$
341.6	299.9(10.4)	591.2	0.29(2)	0.96(6)	0.83(8)	$15/2^-,7/2 \rightarrow 11/2^-,7/2$
346.9	12.8(9)	3229.2	0.46(11)		0.89(22)	$35/2^-,25/2 \rightarrow 33/2^-,25/2$
348.6	9.8(1.2)	3222.3				$(31/2^+,29/2) \rightarrow (29/2^+,29/2)$
351.9	25.7(1.5)	3217.9			0.82(15)	$35/2^+,23/2 \rightarrow 33/2^+,23/2$
357.1	32.2(2.0)	2070.5				$(23/2^-,23/2) \rightarrow (25/2^-,25/2)$
359.8	76.5(3.7)	3466.6	0.17(8)		1.14(20)	$41/2^+,39/2 \rightarrow 39/2^+,39/2$
360.1	5.8(0.9)	3582.1				$(33/2^+,29/2) \rightarrow (31/2^+,29/2)$
361.7	14.1(1.0)	3579.6	0.40(12)			$37/2^+,23/2 \rightarrow 35/2^+,23/2$
363.7	13.6(1.2)	(1205.2)				$(17/2^-,1/2) \rightarrow (13/2^-,1/2)$
364.0	16.9(1.1)	2700.6				$(29/2^-,23/2) \rightarrow (25/2^-,23/2)$
364.6	7.9(1.0)	3593.6				$37/2^-,25/2 \rightarrow 35/2^-,25/2$
365.7	85.1(4.0)	3106.7	−0.06(3)		0.55(6)	$39/2^+,39/2 \rightarrow 37/2^-,37/2$
366.2	28.9(1.6)	2615.7				$(27/2^-,23/2) \rightarrow 29/2^-,25/2$
366.5	11.8(1.8)	(3304.0)				$(35/2^-,33/2) \rightarrow (33/2^-,33/2)$
368.0	67.3(2.7)	2336.3	0.32(6)		0.89(9)	$(25/2^-,23/2) \rightarrow 29/2^-,25/2$
369.4	8.5(0.9)	3949.0				$39/2^+,25/2 \rightarrow 37/2^+,25/2$
375.1	37.0(1.9)	3841.8	0.25(3)		0.95(14)	$43/2^+,39/2 \rightarrow 41/2^+,39/2$
378.4	153.0(5.2)	1086.6				$19/2^+,9/2 \rightarrow 15/2^+,9/2$
383.3	6.5(1.0)	(3687.4)				$(37/2^-,33/2) \rightarrow (35/2^-,33/2)$
384.9	262.1(9.0)	794.2	0.25(2)	0.95(7)	0.97(9)	$17/2^-,7/2 \rightarrow 13/2^-,7/2$
391.3	17.0(1.2)	4233.1			1.23(25)	$45/2^+ 39/2 \rightarrow 43/2^+,39/2$
391.6	22.6(1.5)	1536.7				$(17/2^-,1/2) \rightarrow (13/2^-,1/2)$
397.7	37.7(2.5)	1713.5	−0.06(5)		0.60(10)	$25/2^-,25/2 \rightarrow 23/2^+,23/2$
401.3	46.3(3.4)	3142.3			1.10(22)	$39/2^-,37/2 \rightarrow 37/2^-,37/2$
407.7	16.0(1.3)	(1566)				$(15/2^-,1/2) \rightarrow (11/2^-,1/2)$
408.1	8.2(0.9)	4641.2				$47/2^+,39/2 \rightarrow 45/2^+,39/2$
418.3	133.8(4.6)	1300.9	0.19(3)	0.93(13)	1.15(13)	$21/2^+,9/2 \rightarrow 17/2^+,9/2$
420.9	37.9(2.7)	3563.3			1.22(25)	$41/2^-,37/2 \rightarrow 39/2^-,37/2$
424.0	0.9(0.7)	3066.0				$49/2^+,39/2 \rightarrow 47/2^+,39/2$
426.3	227.1(7.8)	1017.5		0.89(5)	1.07(15)	$19/2^-,7/2 \rightarrow 15/2^-,7/2$
440.0	13.5(1.9)	4003.2			1.12(33)	$43/2^-,37/2 \rightarrow 41/2^-,37/2$
441.6	16.8(1.3)	2409.8				$(27/2^-,23/2) \rightarrow 27/2^-,25/2$
448.1	7.4(0.9)	(1653.3)				$(21/2^-,1/2) \rightarrow (17/2^-,1/2)$
450.8	5.6(1.1)	2418.6				$(29/2^-,23/2) \rightarrow 29/2^-,25/2$
458.0	3.2(1.1)	4461.0				$45/2^-,37/2 \rightarrow 43/2^-,37/2$
465.7	180.8(6.3)	1259.9	0.15(3)	0.81(5)	1.01(13)	$21/2^-,7/2 \rightarrow 17/2^-,7/2$
470.2	17.2(1.2)	2005.1				$(21/2^-,1/2) \rightarrow (17/2^-,1/2)$
474.4	92.1(3.3)	1560.9	0.15(3)	1.03(14)	1.26(16)	$23/2^+,9/2 \rightarrow 19/2^+,9/2$
483.6	16.9(1.2)	(2049)				$(19/2^-,1/2) \rightarrow (15/2^-,1/2)$
501.6	83.3(3.1)	1802.6		0.83(12)	0.95(14)	$25/2^+,9/2 \rightarrow 21/2^+,9/2$
502.9	156.2(5.5)	1520.4		0.87(5)		$23/2^-,7/2 \rightarrow 19/2^-,7/2$
503.4	7.0(3.7)	1846.1				$23/2^-,19/2 \rightarrow 19/2^-,19/2$
508.1	6.9(1.6)	508.1				$5/2^-,5/2 \rightarrow 7/2^-,7/2$
526.1	4.0(0.7)	(2179.4)				$(25/2^-,1/2) \rightarrow (21/2^-,1/2)$
534.0	8.4(0.9)	2539.1				$(25/2^-,1/2) \rightarrow (21/2^-,1/2)$
536.3	21.1(1.6)	2249.6				$29/2^-,25/2 \rightarrow 25/2^-,25/2$
537.9	112.4(4.1)	1797.8	0.27(3)	0.95(7)	0.86(22)	$25/2^-,7/2 \rightarrow 21/2^-,7/2$
541.0	10.6(1.8)	2124.3				$25/2^-,19/2 \rightarrow 21/2^-,19/2$
541.6	7.1 (0.9)	(2591)				$(23/2^-,1/2) \rightarrow (19/2^-,1/2)$
567.1	50.0(2.1)	2128.1				$27/2^+,9/2 \rightarrow 23/2^+,9/2$
570.4	86.4(3.3)	2090.8		1.02(7)		$27/2^-,7/2 \rightarrow 23/2^-,7/2$

TABLE I. (*Continued*).

E_γ(keV)	I_γ	E_{level}(keV)	A_2/A_0	$R_{\Delta J=2}$	$R_{\Delta J=1}$	$(J^\pi,K)_i \rightarrow (J^\pi,K)_f$
570.5	10.5(1.6)	2416.8				$27/2^-,19/2 \rightarrow 23/2^-,19/2$
572.3	25.5(3.3)	1888.0				$27/2^+,23/2 \rightarrow 23/2^+,23/2$
575.0	46.7(2.1)	2377.6		0.87(28)	0.73(16)	$29/2^+,9/2 \rightarrow 25/2^+,9/2$
586.7	27.7(1.7)	2555.1			0.72(17)	$31/2^-,25/2 \rightarrow 27/2^-,25/2$
594.4	4.0(0.7)	3133.5				$(29/2^-,1/2) \rightarrow (25/2^-,1/2)$
600.5	13.7(1.7)	2724.8				$29/2^-,19/2 \rightarrow 25/2^-,19/2$
600.9	71.0(2.8)	2398.7		1.17(10)		$29/2^-,7/2 \rightarrow 25/2^-,7/2$
606.3	43.7(3.0)	2199.5				$29/2^+,23/2 \rightarrow 25/2^+,23/2$
623.1	19.7(1.6)	2336.3				$(25/2^-,23/2) \rightarrow 25/2^-,25/2$
628.9	40.0(1.9)	2719.7		1.41(16)		$31/2^-,7/2 \rightarrow 27/2^-,7/2$
630.5	5.7(1.3)	3047.8				$31/2^-,19/2 \rightarrow 27/2^-,19/2$
632.6	25.2(1.5)	2882.4			0.77(17)	$33/2^-,25/2 \rightarrow 29/2^-,25/2$
637.8	30.1(2.2)	2525.9				$31/2^+,23/2 \rightarrow 29/2^+,23/2$
637.8	20.9(1.3)	3015.4		1.27(28)	1.12(39)	$33/2^+,9/2 \rightarrow 29/2^+,9/2$
647.1	17.7(1.5)	2615.7				$(27/2^-,23/2) \rightarrow 27/2^-,25/2$
654.6	14.6(1.2)	2782.7		0.95(17)		$31/2^+,9/2 \rightarrow 27/2^+,9/2$
654.6	22.7(1.4)	3053.3		0.71(20)	0.87(36)	$33/2^-,7/2 \rightarrow 29/2^-,7/2$
659.6	7.7(1.1)	2909.3				$(29/2^-,23/2) \rightarrow 29/2^-,25/2$
662.9	9.8(1.0)	3217.8				$(31/2^-,23/2) \rightarrow 31/2^-,25/2$
666.2	16.9(1.5)	2865.9			1.36(42)	$33/2^+,23/2 \rightarrow 29/2^+,23/2$
674.2	14.9(1.1)	3229.2			0.70(14)	$35/2^-,25/2 \rightarrow 31/2^-,25/2$
674.2	5.4(1.2)	2873.7				$(29/2^+,29/2) \rightarrow 29/2^+,23/2$
678.8	13.5(1.1)	3398.4		1.04(19)		$35/2^-,7/2 \rightarrow 31/2^-,7/2$
687.6	4.7(0.8)	3703.0		1.16(36)		$37/2^+,9/2 \rightarrow 33/2^+,9/2$
691.8	9.4(1.2)	3217.9			0.77(21)	$35/2^+,23/2 \rightarrow 31/2^+,23/2$
696.0	10.8(1.3)	2409.8				$(27/2^-,23/2) \rightarrow 25/2^-,25/2$
700.0	8.2(0.9)	3753.3		0.77(23)		$37/2^-,7/2 \rightarrow 33/2^-,7/2$
(709.6)	<2	3582.1				$(33/2^+,29/2) \rightarrow (29/2^+,29/2)$
711.2	9.1(1.0)	3593.6			1.23(34)	$37/2^-,25/2 \rightarrow 33/2^-,25/2$
713.6	4.9(1.0)	3579.6				$37/2^+,23/2 \rightarrow 33/2^+,23/2$
730.7	4.2(0.9)	3949.0				$39/2^+,23/2 \rightarrow 35/2^+,23/2$
722.2	2.0(0.7)	4120.6				$39/2^-,7/2 \rightarrow 35/2^-,7/2$
734.7	2.2(0.8)	3517.3		1.11(49)		$35/2^+,9/2^+ \rightarrow 31/2^+,9/2$
734.9	8.6(1.6)	3841.8				$43/2^+,39/2 \rightarrow 39/2^+,39/2$
744.1	0.8(0.6)	4497.4				$41/2^-,7/2 \rightarrow 37/2^-,7/2$
(753.4)	<1	(3687.4)				$(37/2^-,33/2) \rightarrow (33/2^-,33/2)$
766.5	8.9(1.3)	4233.1				$45/2^+,39/2 \rightarrow 41/2^+,39/2$
799.6	5.3(1.0)	4641.2				$47/2^+,39/2 \rightarrow 43/2^+,39/2$
823.0	11.4(5.5)	3563.3				$41/2^-,37/2 \rightarrow 37/2^-,37/2$
833.1	3.3(1.0)	5066.0				$49/2^+,39/2 \rightarrow 45/2^+,39/2$
860.5	8.4(2.0)	4003.2				$43/2^-,37/2 \rightarrow 39/2^-,37/2$
897.1	0.4(4)	4461.2				$45/2^-,37/2 \rightarrow 41/2^-,37/2$
985.6	13.9(1.9)	2873.7				$(29/2^+,29/2) \rightarrow 27/2^+,25/2$

three angles in the CAESAR array. Fits to these spectra enabled the extraction of intensities for most of the strongest and uncontaminated transitions. These were used to generate the angular distributions to which the second-order function

$$W(\Theta) = A_0[1 + A_2 P_2(\Theta)]$$

was fitted. The resultant A_2 coefficients are listed in Table I.

IV. CONFIGURATION ASSIGNMENTS

The in-band branching ratios

$$\lambda = \frac{I_\gamma(J \rightarrow J-2)}{I_\gamma(J \rightarrow J-1)}$$

were used to determine the mixing ratio (δ) for the $\Delta J = 1$ cascade transitions from which the ratio of the intrinsic gy-

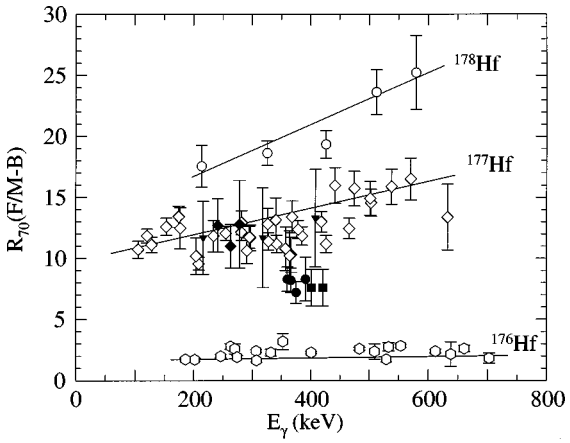

FIG. 4. ''Forward/Middle-Back'' intensity ratios (see text) for known bands in ^{176}Hf, ^{177}Hf, and ^{178}Hf (open symbols) together with those for new bands in ^{177}Hf (filled symbols) which could not be connected via γ-γ coincidences. Triangles: $K^\pi = 1/2^-$; diamonds: $K^\pi = 19/2^-$; squares: $K^\pi = 37/2^-$; circles: $K^\pi = 39/2^+$. No efficiency correction has been applied to the ratios. The lines are drawn to guide the eye.

romagnetic ratio (g_K) to the intrinsic quadrupole moment (Q_0) was calculated according to rotational model formulas:

$$\frac{\delta^2}{1+\delta^2} = \frac{2K^2(2J-1)}{(J+1)(J-1+K)(J-1-K)} \times \frac{E^5_{\gamma,\Delta J=1}}{E^5_{\gamma,\Delta J=2}} \times \lambda, \tag{1}$$

$$\frac{g_K - g_R}{Q_0} = \frac{0.933 E_{\gamma,\Delta J=1}}{\delta\sqrt{J^2-1}}. \tag{2}$$

Equation (1) is derived in the strong-coupling limit, and hence assumes that the value of K is well defined, which is an approximation when Coriolis mixing is non-negligible. Since Eq. (1) yields only the magnitude of δ, the sign of δ was determined, where possible, from the sign of the A_2 coefficient. The values of $(g_K - g_R)/Q_0$ that were derived from Eq. (2) are shown in Table II.

A. Bands based on one-quasiparticle states

1. The 7/2$^-$[514] ground-state band

The band based on the $K^\pi = 7/2^-$ stable ground state was previously observed up to the $27/2^-$ level [12]. It has now been extended to the $41/2^-$ state, as can be seen in Fig. 1. A sum-of-gates spectrum is shown in Fig. 5(a). The angular distribution data indicate that the weak $\Delta J = 1$ cascade transitions have negative A_2 coefficients. Since the $M1$ transition strength is low for this configuration, the branching ratios are large, and the $\Delta J = 1$ cascade transitions are not observed above the $19/2^-$ level. The measured branching ratios suggest $(|g_K - g_R|)/Q_0 < 0.01$, so that $g_K \simeq g_R = 0.23(2)$, where the value g_R was taken from the g-factor measurements of Ref. [13]. This is in reasonable agreement with the Nilsson estimate of $g_K = 0.26$ for deformation of $\varepsilon_2 = 0.245$, as derived from the measured quadrupole moment [14]. The alignment plot (Fig. 7) shows evidence for a gradual rotational alignment, most likely due to a pair of $i_{13/2}$ neutrons. No signature splitting is observed.

2. The 9/2$^+$[624] band

The band based on the $9/2^+$ intrinsic state at 321.2 keV has been extended from $J^\pi = 23/2^+$ [12] to $J^\pi = 37/2^+$. A coincidence spectrum for the band is shown in Fig. 5(b). Large, negative A_2 coefficients were obtained for several of the cascade transitions. Hence, a negative sign was chosen for $(g_K - g_R)/Q_0$. The mean value of g_K extracted was $-0.142(23)$, which deviates significantly from the simple Nilsson estimate of -0.245. This is most likely due to Coriolis-induced K mixing, as observed in the isotone ^{179}W [15], where a value of $g_K(9/2^+) = 0.08(6)$ was found. The deviation from the Nilsson estimate is not so great in ^{177}Hf, which signifies that the K mixing is less severe than in ^{179}W. This is probably due to the larger ε_4 deformation in ^{179}W, which tends to compress spacing of the low-Ω members of the $i_{13/2}$ multiplet, leading to increased K mixing.

The K mixing is also evident in the large signature splitting, which increases monotonically with rotational frequency, as can be seen in Fig. 7. Closer inspection of the extracted values of $(g_K - g_R)/Q_0$ shows that they oscillate with the signature splitting, with the unfavored band members exhibiting higher values.

3. Decoupled bands based on the $\nu 1/2^-[510]$ and $\nu 1/2^-[521]$ orbitals

Three decoupled bands were found that did not show coincidences with known transitions in any hafnium isotope. The F/(M-B) intensity ratios for two of the bands suggest that they should be assigned to ^{177}Hf; the ratios for the third band were lower, so that its assignment to ^{177}Hf is on this basis is tentative. It is the most strongly populated of the three, however, and the energy of the lowest transition [$E_\gamma = 176.5$ keV] matched the energy-spacing of $9/2^-$ and $5/2^-$ levels ($\Delta E = 174(8)$ keV) assigned to the $\nu 1/2^-[510]$ orbital from light-ion transfer measurements [16]. Also, it did not correspond to any decoupled band known to belong to another nucleus that was present in the data. The $1/2^-$ bandhead was not explicitly observed in the transfer data, but its excitation energy ($\sim$567 keV) was inferred from a rotational-model fit to the higher levels assigned to the band. No evidence was seen in the present data for the $\sim$100 keV $5/2^- \rightarrow 1/2^-$ transition implied by the transfer data, which, if it carried the full intensity of the higher transition, should have been observed. This may indicate that the $\Delta J = 1$ transitions dominate at the bottom of the band. Since the expected transition energies are low ($\sim$57 keV for $5/2^- \rightarrow 3/2^-$, and $\sim$41 keV for $3/2^- \rightarrow 1/2^-$), they would not have been observed under the present conditions, due to electron conversion.

Since the only other low-lying $K = 1/2$ orbital is the $\nu 1/2^-[521]$ Nilsson state, the other two decoupled bands are assigned as signature partners based on this orbital. The transfer data suggest that this orbital resides at an excitation energy of 559 keV, while in the isotone ^{179}W it is located at 222 keV, which is $\sim$400 keV lower than the $\nu 1/2^-[510]$ state. The stronger of the two bands in ^{177}Hf is probably the favored positive-signature sequence. Comparison with the analogous bands in ^{179}W suggests that the lowest energy γ

TABLE II. Configurations, branching ratios, mixing ratios, $B(M1)/B(E2)$ ratios and values of $|(g_K-g_R)/Q_0|$ for rotational bands in ^{177}Hf.

Config^n J_i^π	$E_\gamma(\Delta J=1)$ keV	$E_\gamma(\Delta J=2)$ keV	λ	$\lvert\delta\rvert$	$B(M1)/B(E2)$ μ_N^2/e^2b^2	$\lvert(g_K-g_R)/Q_0\rvert$
$7/2^-[514]$						
$11/2^-$	136.6	249.6	5.31(48)	2.30(21)	0.02(1)	0.0103(9)
$13/2^-$	159.6	296.5	11.55(73)	2.79(18)	0.03(1)	0.0083(5)
$15/2^-$	181.8	341.6	18.45(1.35)	4.02(29)	0.03(1)	0.0057(4)
$17/2^-$	203.0	384.9	26.05(2.38)	14.85(1.36)	0.03(1)	0.0015(1)
$19/2^-$	223.3	426.3	37.82(4.65)	5.10(63)	0.02(1)	0.0043(5)
$9/2^+[624]$						
$13/2^+$	128.4	233.8	0.38(2)	0.38(1)	0.52(3)	0.0493(14)
$15/2^+$	153.1	281.1	0.86(4)	0.38(1)	0.35(1)	0.0510(14)
$17/2^+$	174.3	327.7	1.41(7)	0.36(1)	0.31(1)	0.0536(14)
$19/2^+$	204.0	378.4	2.23(11)	0.40(1)	0.25(1)	0.0507(14)
$21/2^+$	214.3	418.3	3.12(17)	0.35(1)	0.26(1)	0.0540(17)
$23/2^+$	260.0	474.4	5.19(36)	0.50(2)	0.15(1)	0.0418(17)
$25/2^+$	241.8	501.6	8.11(72)	0.40(2)	0.17(1)	0.0456(21)
$27/2^+$	325.4	567.1	8.23(1.62)	0.61(7)	0.11(2)	0.0368(42)
$29/2^+$	249.4	575.0	9.70(1.71)	0.27(2)	0.27(4)	0.0596(47)
$K^\pi=19/2^-$						
$23/2^-$	263.0	503.0	0.13(7)	0.30(6)	8.4(4.0)	$0.51(^{+9}_{-14})$
$25/2^-$	278.3	540.9	0.41(8)	0.36(3)	3.24(61)	0.419(39)
$27/2^-$	292.8	570.6	0.84(16)	0.41(4)	1.71(35)	0.352(36)
$29/2^-$	308.1	600.5	1.16(20)	0.41(4)	1.37(25)	0.345(36)
$31/2^-$	323.5	630.6	1.0(3)	0.33(5)	1.85(57)	$0.427(^{+60}_{-70})$
$K^\pi=23/2^+$						
$27/2^+$	295.1	572.3	0.13(2)	0.31(2)	12.1(1.6)	0.0631(40)
$29/2^+$	311.5	606.3	0.34(3)	0.36(2)	4.87(41)	0.0535(22)
$31/2^+$	326.5	637.8	0.38(3)	0.30(1)	5.07(44)	0.0635(28)
$33/2^+$	340.1	666.2	0.42(4)	0.26(1)	5.19(55)	0.0708(38)
$35/2^+$	351.9	691.8	0.36(5)	0.21(1)	6.66(90)	0.0858(57)
$37/2^+$	361.7	713.6	0.35(7)	0.18(2)	7.5(1.5)	$0.0961(^{+86}_{-103})$
$39/2^+$	369.4	730.7	0.50(12)	0.20(2)	5.6(1.4)	$0.0860(^{+93}_{-113})$
$K^\pi=25/2^-$						
$29/2^-$	281.4	536.4	0.14(1)	0.37(2)	8.79(77)	0.0476(21)
$31/2^-$	305.4	586.7	0.39(3)	0.43(2)	3.73(30)	0.0417(17)
$33/2^-$	327.3	632.6	0.81(6)	0.50(2)	1.99(19)	0.0356(17)
$35/2^-$	346.9	674.2	1.16(12)	0.51(3)	1.59(20)	0.0351(22)
$37/2^-$	364.6	711.1	1.16(19)	0.43(4)	1.90(37)	0.0413(40)
$K^\pi=(29/2^+)$						
$(33/2^+)$	360.1	709.6	0.31(31)	0.60(38)	6(14)	$0.24(^{+10}_{-39})$
$K^\pi=(33/2^-)$						
$(37/2^-)$	383.3	753.4	0.17(17)	0.45(26)	15(39)	$0.31(^{+11}_{-42})$
$K^\pi=37/2^-$						
$41/2^-$	420.9	823.0	0.30(15)	0.74(23)	7.6(5.2)	$0.0253(^{+65}_{-97})$
$43/2^-$	440.0	860.5	0.62(17)	0.74(16)	4.0(1.7)	0.0249(51)
$K^\pi=39/2^+$						
$43/2^+$	375.1	734.9	0.23(5)	0.63(7)	8.6(2.1)	$0.0249(^{+26}_{-31})$
$45/2^+$	391.3	766.5	0.52(8)	0.68(7)	4.02(89)	0.0232(25)
$47/2^+$	408.1	799.6	0.64(15)	0.58(9)	3.9(1.2)	0.0271(39)

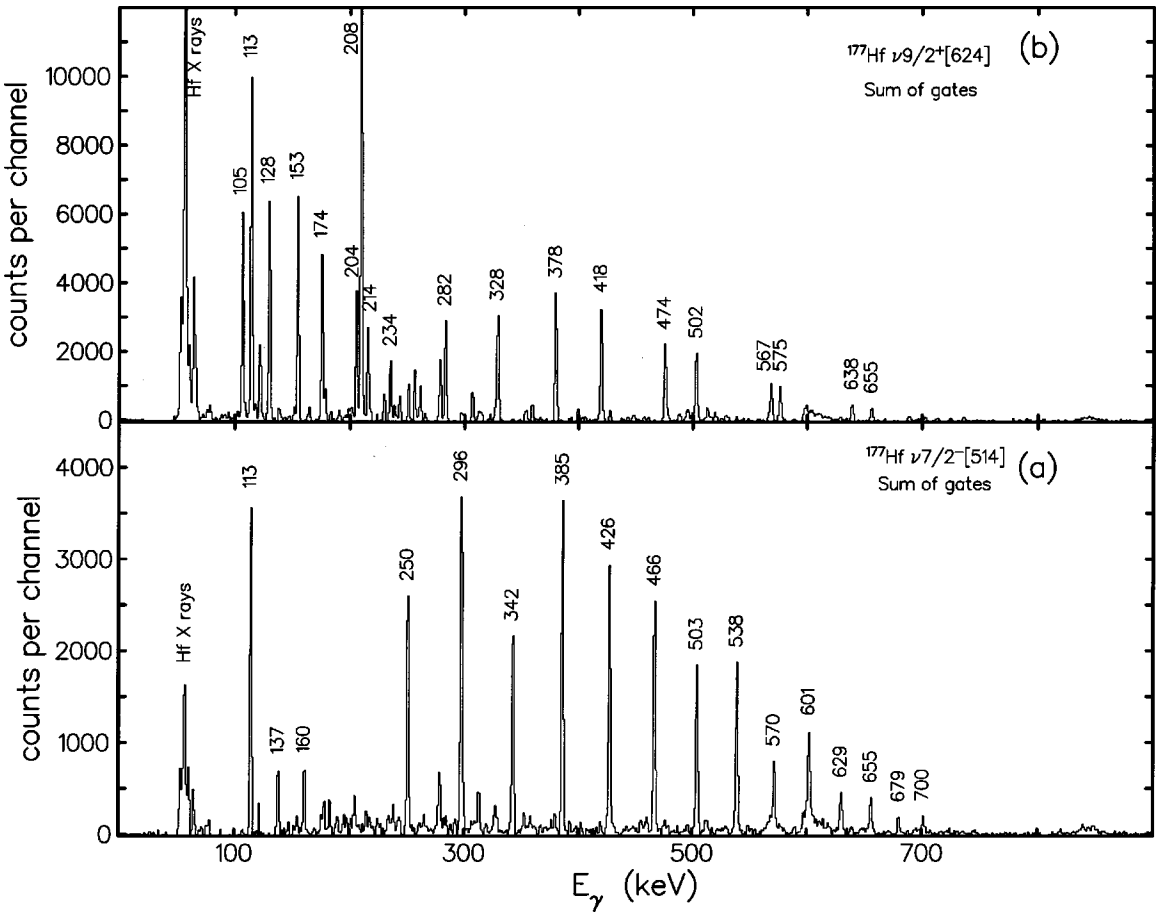

FIG. 5. (a) Coincidence spectrum generated by summing gates set on members of the $\nu 7/2^-$ ground-state band. (b) Coincidence spectrum generated by summing gates set on members of the $\nu 9/2^+$ band.

ray (194 keV) in the favored signature is the $9/2^- \rightarrow 5/2^-$ transition. Similarly the 216 keV γ ray is assigned as the $7/2^- \rightarrow 3/2^-$ transition in the unfavored signature sequence. If these spin assignments are correct, then the alignments (Fig. 7) resemble those of the analogous bands in ^{179}W [15].

It should be noted that neither of the γ-ray energies mentioned above match the spacing of any pair of levels assigned as members of the $1/2^-[521]$ band from the (d,p) and (d,t) data. Also, there is no evidence for the 93 keV $5/2^- \rightarrow 1/2^-$ or the 65 keV $3/2^- \rightarrow 1/2^-$ transitions, which would be expected from the (d,p) data. It is possible that the proximity of the two $K^\pi = 1/2^-$ and associated states in ^{177}Hf leads to a fragmentation of decay at the bottom of all three decoupled bands. The decay from the $K^\pi = 1/2^-$ bandheads could not be established, even though previous measurements suggest a 51 keV $E2$ decay from the $\nu 1/2^-[521]$ state to the $\nu 5/2^-[512]$ bandhead.

4. The $\nu 5/2^-[512]$ band

Evidence was found for population of the band based on the $\nu 5/2^-[512]$ second excited state located at an excitation energy of 508.1 keV [16–18]. Since this level is highly nonyrast, the associated rotational band was populated very weakly, so that only the $7/2^-$ and $9/2^-$ members were identified.

B. Bands based on three-quasiparticle states

1. The band based on the $K^\pi = 23/2^+$, $T_{1/2} = 1.1$ s isomer

The $K^\pi = 23/2^+$ state is a well-known isomer with $T_{1/2} = 1.1$ s. It was first observed from the β-decay of the $K^\pi = 23/2^-$, $T_{1/2} = 161$ day isomer in ^{177}Lu [1,2]. Later measurements were able to establish its associated band up to $J^\pi = 31/2^+$ [3]. This has been extended to $J^\pi = 39/2^+$ in the present work. The band is displayed in Fig. 6(a), where a spectrum gated by the 277 keV transition is shown. The average value of g_K (see Table III) extracted from the first four branchings in the band agrees well with the previously suggested three-quasiparticle configuration for the $K^\pi = 23/2^+$ state was $\pi^2[7/2^+ 9/2^-]8^- \otimes \nu 7/2^-$. Beyond this, the value g_K increases, probably due to the rotational alignment of $i_{13/2}$ neutrons, for which evidence is seen in the net alignment for the band shown in Fig. 7.

2. The band based on the $K^\pi = 25/2^-$ state

The existence of the $K^\pi = 25/2^-$ state had previously been established from the observation of its decay to the $25/2^+$ member of the $K^\pi = 23/2^+$ band via the 120 keV unstretched $E1$ transition [19], which can be seen in Fig. 6(a). The cascade transition from the $27/2^-$ member of the associated band had been firmly assigned, together with tentative cascade/crossover candidates from the $29/2^-$ rotational level. The band is established to $J^\pi = 37/2^-$ in the present work.

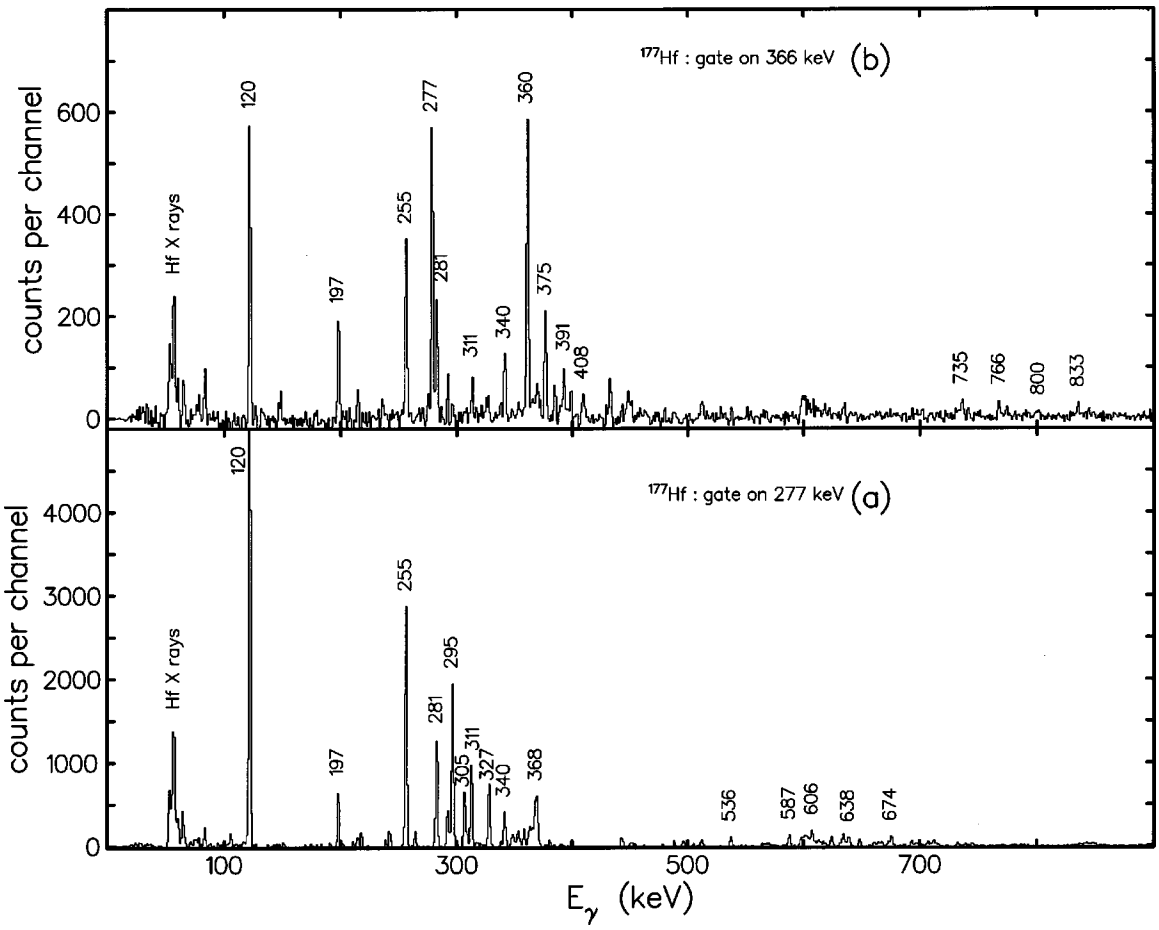

FIG. 6. (a) Coincidence spectrum generated by gating on the 277 keV transition in ^{177}Hf. Members of the bands based on the $K^\pi = 23/2^+$ and $K^\pi = 25/2^-$ three-quasiparticle states can be seen. (b) Coincidence spectrum generated by gating on the 366 keV transition in ^{177}Hf. Members of the bands based on the $K^\pi = 39/2^+$ five-quasiparticle state can be seen. Since the 366 keV transition is a multiplet, transitions associated with the $K^\pi = 23/2^+$ and $K^\pi = 25/2^-$ states are also present in the spectrum.

TABLE III. Configurations and g_K factors for multiquasiparticle states in ^{177}Hf.

	Configuration[a]		g_K		
K^π	ν	π	Exp[b]	Nilsson[c]	Empirical[d]
$7/2^-$	$7/2^-$		0.23(2)	0.26	0.23(2)
$9/2^+$	$9/2^+$		−0.142(23)	−0.245	−0.142(23)
$19/2^-$	$7/2^-$	$7/2^+$,$5/2^+$	0.64(5)	0.74	0.72
			0.71(5)†		
$23/2^+$	$7/2^-$	$7/2^+$,$9/2^-$	0.68(4)	0.79	0.77
			0.75(4)†		
$25/2^-$	$9/2^+$	$7/2^+$,$9/2^-$	0.52(4)	0.55	0.59
			0.59(4)†		
$(29/2^+)$	$7/2^-$	$1/2^+$, $5/2^+$, $7/2^+$, $9/2^-$	$0.54(^{+10}_{-29})$	0.60	0.60
$(33/2^-)$	$1/2^-$, $7/2^-$, $9/2^+$	$7/2^+$, $9/2^-$	$0.54(^{+11}_{-42})$	0.50	0.52
$37/2^-$	$5/2^-$, $7/2^-$, $9/2^+$	$7/2^+$, $9/2^-$	0.41(3)	0.38	0.40
$39/2^+$	$7/2^+$, $7/2^-$, $9/2^+$	$7/2^+$, $9/2^-$	0.41(2)	0.36	0.40

[a] π: $7/2^+$: $7/2^+[404]$; $9/2^-$: $9/2^-[514]$; $5/2^+$: $5/2^+[402]$; $1/2^+$: $1/2^+[411]$. ν: $9/2^+$: $9/2+[624]$; $7/2^-$: $7/2^-[514]$; $5/2^-[512]$; $7/2^+$: $7/2^+[633]$; $1/2^-$: $1/2^-[510]$.

[b] $(g_K - g_R)/Q_0$ is positive (except for $7/2^-$ and $9/2^+$), $Q_0 = 7.2(1)$ eb (Ref. [14]), $g_R = 0.23(2)$ †, $g_R = 0.3$).

[c] Nilsson wave functions, $g_s = 0.7 g_{\text{free}}$ and deformations of $(\varepsilon_2, \varepsilon_4) = (0.245, 0.053)$.

[d] Empirical g_K values used wherever possible.

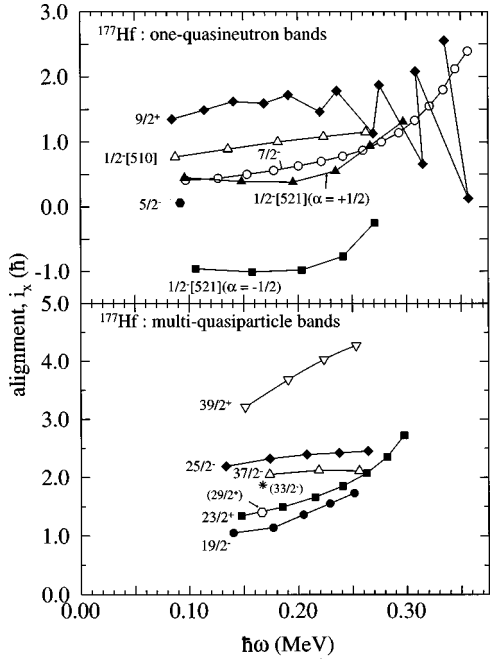

FIG. 7. Aligned angular momenta for bands in ^{177}Hf, extracted with K values as shown in the figure. The Harris reference parameters used were $\mathcal{J}_0 = 36\,\hbar^2/\mathrm{MeV}$ and $\mathcal{J}_1 = 76\,\hbar^4/\mathrm{MeV}^3$.

Also, the 398 keV stretched $E1$ transition from the bandhead directly to the $K^\pi = 23/2^+$ state has been found, but it is weak compared to the 120 keV $J \rightarrow J$ transition. This behavior reflects that of the well-known $E1$ branchings from the $\nu 9/2^+$ band to the $\nu 7/2^-$ band [20] in ^{177}Hf, since the $25/2^-$ and $23/2^+$ configurations correspond to coupling these two orbitals to the same $\pi^2 8^-$ component, respectively.

The average value of g_K for the band (see Table III) agrees well with that expected for the previously suggested configuration of $\pi^2[7/2^+,9/2^-] \otimes \nu 9/2^+$. Further evidence comes from the alignment plot (Fig. 7), which shows that the band has more aligned spin than that based on the $K^\pi = 23/2^+$ state, consistent with the occupancy of the $\nu i_{13/2},9/2^+$ orbital. The presence of the latter quasiparticle also blocks the $\nu i_{13/2}$ alignment that is observed in the $K^\pi = 23/2^+$ band.

3. The band based on the $K^\pi = 19/2^-$, $T_{1/2} = 56\,\mu$s isomer

In a previous study of ^{177}Hf, a $K^\pi = 19/2^-$ state with a half-life of 56 μs was found [19]. This was assigned to the $\nu 7/2^- \otimes \pi^2[7/2^+,5/2^+]6^+$ three-quasiparticle configuration. The present experimental conditions precluded the observation of the 548 keV transition from the $K^\pi = 19/2^-$ state to the $17/2^-$ state of the $\nu 7/2^-$ band. Moreover, the lifetime prohibits the use of early-delayed coincidence techniques as means with which to assign the band associated with the $K^\pi = 19/2^-$ state. Hence, the band will be decoupled in prompt and delayed coincidence from the $\nu 7/2^-$ band. A band was found which had similar level energies to that of the $\nu 7/2^-$ band above the $19/2^-$ state, but with strong $\Delta J = 1$ cascade transitions. It could not be connected via γ-γ coincidences with any of the hafnium level schemes. The F/(M-B) intensity ratios for the band are depicted by the filled diamonds in Fig. 4, which clearly indicate that the band should be assigned to ^{177}Hf. The values of g_K extracted from the branching ratios (Table III) are in good agreement with those expected for the $\nu 7/2^- \otimes \pi^2 6^+$ configuration. Hence, this band has been assigned to the $K^\pi = 19/2^-$ three-quasiparticle state.

The alignments show a similar behavior to those of the $23/2^+$ band, but are $\sim 0.3\hbar$ lower. This is consistent with the difference in alignment between the $\pi^2 6^+$ and dominantly $\pi^2 8^-$ bands in ^{178}Hf [4]. As in the $23/2^+$ band, the smooth increase in aligned spin is attributed to the alignment of a pair of $i_{13/2}$ neutrons.

4. Bands based on $K^\pi = (23/2^-)$ states

There are a number of states that decay into the levels of the $25/2^-$ band, as shown in Fig. 3. The spacing between these states suggests that they could constitute a rotational band in which the in-band transitions are very weak. Since no decay is observed to members of the $23/2^+$ band, the new states probably have negative parity, and their energy spacing suggests that they are based on a three-quasiparticle structure. There are also a number of other states that decay into this structure and also to the $25/2^-$ band. This suggests that there may be at least two bands which are strongly mixed with one another and with the $25/2^-$ band. Multiquasiparticle calculations (see Sec. V B) predict three close-lying $K^\pi = 23/2^-$ states at an excitation energy of ~ 2 MeV. One of these is based on the $\nu 9/2^+ \pi^2\,[5/2^+,9/2^-]$ configuration, which corresponds to exchanging the $\pi 7/2^+[404]$ orbital in the $25/2^-$ configuration for its $\pi 5/2^+[402]$ pseudospin partner. This assignment is consistent with the strong decays into the $25/2^-$ band. A second $23/2^-$ state is based on the $\nu 7/2^+ \pi^2\,[7/2^+,9/2^-]$ configuration. This can couple to the first $23/2^-$ state in two ways; it has the $\pi 7/2^+$ pseudospin partner to the $\pi 5/2^+$ orbital, and the $\nu i_{13/2},7/2^+$ orbital, which will couple to the $\nu i_{13/2},9/2^+$ orbital in the first $23/2^-$ configuration. The third $23/2^-$ state is based on the $\nu^3\,[7/2^+,9/2^+,7/2^-]$ configuration, which has both $\nu i_{13/2}$ orbitals occupied, and may therefore couple with the other two $23/2^-$ states.

C. Bands based on five-quasiparticle states

The only previously known five-quasiparticle state in ^{177}Hf was the $K^\pi = 37/2^-$, $T_{1/2} = 51$ min isomer. It was identified from its decay via a 214 keV $E3$ transition to the $31/2^+$ state of the $23/2^+$ band [3,21]. Since the observed $37/2^-$ state in the band based on the $7/2^-$ ground state resides ~ 1 MeV above the $K^\pi = 37/2^-$ five-quasiparticle state, it seems very likely that the band on the latter should also be populated. Two of the new bands that were assigned to ^{177}Hf on the basis of their F/(M-B) ratios (corresponding to the filled squares and circles in Fig. 4) have cascade-transition energies which strongly suggest that they are associated with five-quasiparticle states. One band is populated with $\sim 60\%$ of the intensity of the other, but they have similar branching ratios. It is also interesting to note that even though the F/(M-B) ratios clearly show that both bands belong to ^{177}Hf, the ratios are lower than the average values for this nucleus (see Sec. V C for further comment on this).

1. The band based on the $K^\pi = 39/2^+$ state at 3107 keV

The stronger of the two bands is in prompt coincidence with a 366 keV transition, which has been assigned as the decay from its band head. Thus, this band *cannot* be the one based on the $K^\pi = 37/2^-$, $T_{1/2} = 51$ min isomer. Instead, it has been assigned to decay to the $K^\pi = 37/2^-$ isomer via the 366 keV transition. A coincidence spectrum gated by the 366 keV transition is shown in Fig. 6(b). Since this band is more intense, it is very likely that it is yrast when compared to the band based on the $K^\pi = 37/2^-$ state, suggesting $K^\pi = 41/2^-$ or $39/2^{(\pm)}$ for the 3107 keV state. Positive A_2 values were found for the 360 and 375 keV cascade transitions, whereas the 366 keV transition has a small negative A_2, consistent with a stretched dipole character. The DCO ratio of the 366 keV transition (when gated by the 360 keV cascade transition) was similar to that of the 398 keV stretched $E1$ transition when gated by the 255 keV cascade in the $23/2^+$ band, supporting stretched dipole character for the 366 keV transition. Hence, this band is assigned to a previously unobserved five-quasiparticle, $K^\pi = 39/2^\pm$ state. There is no indication of mutual perturbation with the close-lying $39/2^-$ member of the band assigned to the $K^\pi = 37/2^-$ state (see below), which favors positive parity. Also, our multiquasiparticle calculations (see Sec. V B) predict that the lowest $K^\pi = 39/2^-$ state resides at $\sim$4.5 MeV, whereas the $\pi^2[7/2^+,9/2^-]8^- \otimes \nu^3[9/2^+,7/2^-,7/2^+]$, $K^\pi = 39/2^+$ configuration occurs at 3.2 MeV. Furthermore, the extracted g_K factor (see Table III) for the band agrees well with that expected for the $K^\pi = 39/2^+$ configuration.

The band has a relatively high alignment, as can be seen in Fig. 7. This is consistent with the occupancy of the two $\nu i_{13/2}$ orbitals ($9/2^+[624]$, $7/2^+[633]$) in the assigned configuration.

2. The band based on the $K^\pi = 37/2^-$, $T_{1/2} = 51$ min isomer

By default, the weaker of the two bands mentioned above was assigned to the $K^\pi = 37/2^-$, $T_{1/2} = 51$ min isomer. It was not possible to extract A_2 coefficients for any of the cascade transitions, but the values of $R_{\Delta J=1}$ of $\sim$1 are similar to those found for the $39/2^+$ band. Hence, the positive sign was taken for $(g_K - g_R)/Q_0$ was taken, and the value extracted for g_K is in good agreement with the empirical estimate.

Despite the two extra particles, the alignment for this five-quasiparticle band is *lower* than that for the related $25/2^-$ three-quasiparticle band. This effect has also been observed in a number of bands in ^{178}Ta, ^{176}Ta, ^{178}W, and ^{179}W, where it has been attributed to the effect of reduced pairing in the higher seniority configuration [22,23]. The reduced pairing apparently lessens the aligned spin contributed by the quasiparticles, but also increases the collective moment of inertia. If the former decreases faster than the latter increases, then the extracted alignment will be lower in the higher seniority configuration, despite the presence of at least two more unpaired particles.

3. The band based on the $K^\pi = (29/2^+)$ state

A weakly populated structure that consists of just two transitions has been observed to decay solely to the $23/2^+$ band via a 986 keV transition, as shown in Fig. 3. The transition energies suggest that the band originates from a five-quasiparticle configuration. Our multiquasiparticle calculations (see Sec. V B) indicate that the $K^\pi = 29/2^+$ $\nu\pi^4$ assignment is most likely, since the decay to the $27/2^+$ state rules out the $31/2^-$ and $33/2^+$ $\nu^3\pi^2$ possibilities. The $\nu\pi^4$ assignment is also consistent with the lack of an $E2$ crossover transition.

4. The band based on the $K^\pi = (33/2^-)$ state

A second weakly populated band was found, which also consisted of just two transitions, both of which were in coincidence with a 197 keV γ ray, but not with any other transitions which are known to belong to a particular hafnium isotope. Reliable F/(M-B) intensity ratios could not be extracted, due to the weakness of the band, but it has been assumed to belong to ^{177}Hf, since it was not observed in the study of ^{178}Hf [4]. The energies of the two inband transitions are consistent with a five-quasiparticle configuration, possibly with $K^\pi = 33/2^\pm$, as suggested by our multiquasiparticle calculations. The $K^\pi = 33/2^-$ assignment would allow the 197 keV transition to be assigned as a decay to the $37/2^-$ isomer, hence the reason for the placement of the band, as shown in Fig. 3. There is little evidence for an $E2$ crossover transition, which is consistent with the calculated g_K value for this configuration.

V. DISCUSSION

A. g_K factors

The overall agreement of the extracted g_K factors with the Nilsson estimates shown in Table III is good, except for the $\nu 9/2^+$ band where considerable K mixing occurs. Not surprisingly, better agreement results when empirical values are used for this orbital and other components in the multiquasiparticle states. It is clear, however, that the g_K values of the $\pi^2\nu$ bands are consistently low, which suggests that the collective g factor (g_R) may be higher for these configurations. Indeed, this appears to be the case for the $\pi^2\nu$, $K^\pi = 25/2^-$ band in ^{179}Hf where the g factor has been measured. The effect is probably due to a reduction in the proton pairing, which is expected to increase g_R by $\sim$0.07 [24]. This suggests that a value of $g_R = 0.3$ is appropriate for the $\pi^2\nu$ bands in ^{177}Hf, which indeed leads to significantly improved agreement between experimental and empirical values of g_K. Clearly it would be of interest to measure the g factors of the $\pi^2\nu$ and $\pi^2\nu^3$ bands in order to gain explicit confirmation of the difference in g_R, since it is not clear why the ground-state value of g_R seems to be appropriate for the $\pi^2\nu^3$ configurations.

In ^{178}Hf and ^{176}Hf there are two 8^- states which arise from the ν^2 $[9/2^+,7/2^-]$ and π^2 $[9/2^-,7/2^+]$ configurations. These configurations are strongly mixed in ^{178}Hf, but are essentially pure in ^{176}Hf. Since the $23/2^+$ and $25/2^-$ states contain the $\nu 7/2^-$ and $\nu 9/2^+$ orbitals, respectively, the Pauli exclusion principle dictates that the 8^- component has to have pure two-quasiproton character. Hence the g_K value for this component should be unity. This can be verified by extracting the g_K for the 8^- component in these two cases; values of 0.98(6) and 1.00(6) were found for the $23/2^+$ and the $25/2^-$ states, respectively.

B. Comparison with blocked multiquasiparticle calculations

Multiquasiparticle calculations were carried out for ^{177}Hf. The prescription used in the calculations followed that out-

TABLE IV. Calculated and observed excitation energies for multiquasiparticle states in ^{177}Hf.

	Configuration		Energy (keV)			
K^π	π	ν	E_{qp}	E_{resid}	E_{calc}	E_{expt}
$7/2^-$		$7/2^-$	0	0	0	0
$9/2^+$		$9/2^+$	350	0	350	321
$5/2^-$		$5/2^-$	530	0	530	508
$1/2^-$		$1/2^-$	576	0	576	(567)
$1/2^-$		$1/2^-$	634	0	634	559
$7/2^+$		$7/2^+$	795	0	795	746
$19/2^-$	$7/2^+,5/2^+$	$9/2^+$	1494	−223	1271	1342
$23/2^+$	$7/2^+,9/2^-$	$7/2^-$	1407	−200	1207	1315
$23/2^-$		$9/2^+,7/2^-,7/2^+$	1999	+14	2013	
$23/2^-$	$5/2^+,9/2^-$	$9/2^+$	2021	+26	2047	
$23/2^-$	$7/2^+,9/2^-$	$7/2^+$	2203	−130	2073	
$25/2^-$	$7/2^+,9/2^-$	$9/2^+$	1757	−129	1627	1713
$29/2^+$	$7/2^+,9/2^-,5/2^+,1/2^+$	$7/2^-$	2832	−94	2738	2874
$31/2^-$	$7/2^+,9/2^-,5/2^+,1/2^+$	$9/2^+$	3182	−56	3125	
$33/2^+$	$7/2^+,5/2^+$	$7/2^-,9/2^+,5/2^-$	3227	−310	2917	
$33/2^-$	$7/2^+,9/2^-$	$7/2^-,9/2^+,1/2^-$	3241	−235	3006	(2938)
$37/2^-$	$7/2^+,9/2^-$	$7/2^-,9/2^+,5/2^-$	3140	−272	2867	2741
$39/2^+$	$7/2^+,9/2^-$	$7/2^-,9/2^+,7/2^+$	3407	−201	3206	3107
$43/2^-$	$7/2^+,9/2^-,5/2^+,1/2^+$	$7/2^-,9/2^+,5/2^-$	4565	−150	4415	
$45/2^+$	$7/2^+,9/2^-,5/2^+,1/2^+$	$7/2^-,9/2^+,7/2^+$	4832	−122	4714	

lined for other cases in this mass region (see, for example, Ref. [25]). More specifically, single-quasiparticle levels were generated from a Nilsson potential at a deformation of $(\varepsilon_2,\varepsilon_4)=(0.256,\ 0.043)$. Pairing correlations were treated within the Lipkin-Nogami approach which included blocking. The energies of the resultant single-quasineutron levels were adjusted to approximately reproduce those known in ^{177}Hf. The single-quasiproton levels were adjusted to those of ^{177}Ta at the same deformation. Fixed pairing strengths of $G_\pi=19.2/A$ MeV and $G_\nu=18.06/A$ MeV were used. Finally, the calculated excitation energies were corrected with an orbital-dependent residual nucleon-nucleon interaction of the form described in Ref. [26].

A comparison between the predicted and observed multiquasiparticle states is given in Table IV. The calculations reproduce the excitation energies of the previously known $K^\pi=19/2^-$, $23/2^+$, $25/2^-$, and $37/2^-$ multiquasiparticle states to within ~100 keV. This is also the case for the newly discovered $K^\pi=39/2^+$ five-quasiparticle state. Hence, an accuracy of ~100 keV can be assumed when attempting to identify other favored configurations.

The comparison shows that the most favored three- and five-quasiparticle states have been observed. There are candidates for some of the less favored intermediate-spin three- and five-quasiparticle states ($K^\pi=23/2^+$, $29/2^+$, $31/2^-$, $33/2^\pm$), but the assignments are tentative. The lowest seven-quasiparticle states (those with $K^\pi=43/2^-$ and $45/2^+$) are predicted to be non-yrast by ~500 keV when compared to the rotational states based on the five-quasiparticle $K^\pi=39/2^+$ state. This can be seen in the lower panel of Fig. 8,

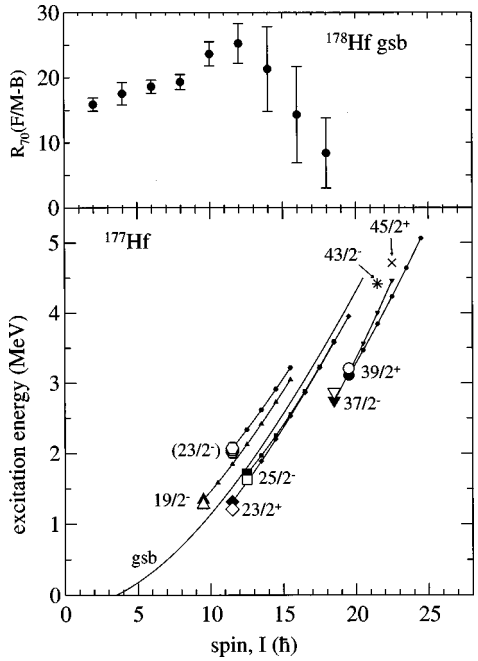

FIG. 8. Lower panel: excitation energy versus spin for states in ^{177}Hf. The experimental (calculated) multiquasiparticle states are depicted by large filled (open) symbols. Associated rotational bands are shown as small filled symbols joined by solid lines. The $43/2^-$ and $45/2^+$ data points correspond to the lowest seven-quasiparticle states predicted by the calculations described in Sec. V B. Upper panel: Forward/(Middle-Back) intensity ratios for the ground-state band in ^{178}Hf, which include data points for the weakly populated top three states (these are not shown in Fig. 9 for clarity of presentation).

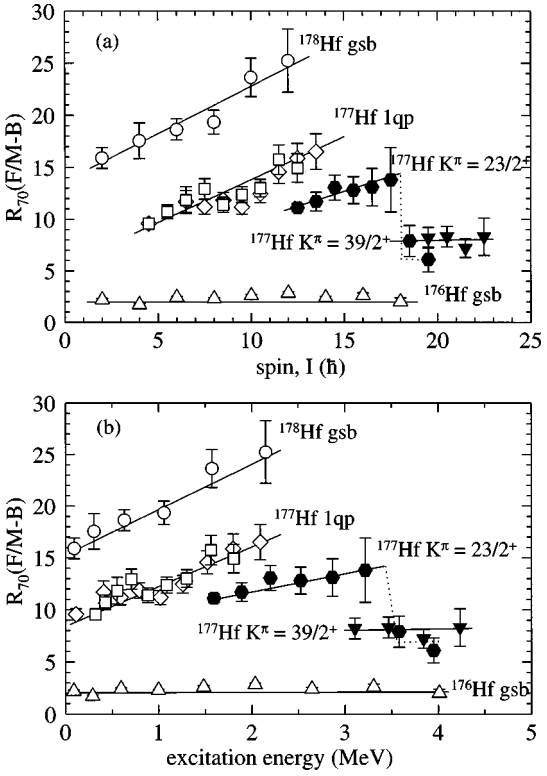

FIG. 9. Forward/(Middle-Back) intensity ratios versus (a) spin, and (b) excitation energy, for the rotational bands in ^{177}Hf based on the ground state, the $K^{\pi}=9/2^{+}$ one-quasineutron state, the $K^{\pi}=23/2^{+}$ three-quasiparticle state and the $K^{\pi}=39/2^{+}$ five-quasiparticle state. Ratios for the ground-state bands in ^{178}Hf and ^{176}Hf are also shown.

where a plot of excitation versus spin is shown for states in ^{177}Hf.

C. Reaction mechanism and spin-population

A previous α-γ study following the bombardment of ^{159}Tb with ^{14}N demonstrated that different intensity profiles for rotational bands resulted if the α particle was detected at forward or backward angles [7]. Rotational bands that were selected by a ''forward'' α particle showed a rapid increase in intensity over the highest spin states, whereupon the intensity remained constant down to the bandhead. This intensity pattern was believed to arise from the narrow spin distribution, localized near to the critical angular momentum for complete fusion, that is associated with incomplete fusion. If the band was selected by a ''backward'' α particle, a gradual monotonic increase in intensity was observed, as expected for complete fusion, where the band is fed over a broad spin range. In the present data, the qualitative behavior of the F/(M-B) intensity ratios as a function of spin can be related to the different entry-spin distributions expected for incomplete fusion and complete fusion. As an example, in the upper panel of Fig. 8 the F/(M-B) ratios for the ground-state band in ^{178}Hf are shown versus spin. A smooth increase with spin is seen up the 12 $\hbar$ state, whereupon a rapid decrease occurs (the large error bars for the top three points are due to the weakness of the relevant γ rays in the M-B matrix). This behavior is consistent with the division of a feeding pattern expected from incomplete fusion by that expected from complete fusion, and suggests that the forward-going α particles tend to be from incomplete fusion, whereas those detected at middle-backward angles are mainly from complete fusion, which is expected to produce an isotropic α distribution in the center-of-mass. The ratios suggest that beyond $\sim$15–20 $\hbar$ the fraction of spin population from incomplete fusion is severely curtailed, and feeding from complete-fusion/evaporation will dominate. This has some consequences for the highest spin states observed in ^{177}Hf, as will be discussed below.

Shown in Fig. 9(a) are F/(M-B) ratios versus spin for rotational bands in ^{177}Hf based on the one-quasiparticle $7/2^{-}$ and $9/2^{+}$ states, the three-quasiparticle $23/2^{+}$ state and the five-quasiparticle $39/2^{+}$ state. The other three- and five-quasiparticle bands in ^{177}Hf are not shown, but they exhibit similar trends to the $23/2^{+}$ and $39/2^{+}$ bands, respectively. These two cases have the best statistical accuracy, and reliable ratios could be extracted up to the highest observed state in each band. For reference, the ratios for the ground-state band (gsb) in ^{178}Hf are shown again, but for clarity of presentation the top three points have been omitted; the ratios for the gsb in ^{176}Hf are also shown. A number of features are noteworthy.

(i) The $7/2^{-}$ gsb and excited $9/2^{+}$ one-quasiparticle bands in ^{177}Hf show a rise with spin similar to that of the gsb in ^{178}Hf. This suggests a similar ratio of population from incomplete fusion and complete fusion to the gsb in ^{178}Hf, as discussed above. It was not possible to extract ratios for the highest bands members in order to ascertain whether a rapid decrease occurs at a spin related to the critical value for complete fusion.

(ii) The ratios for the three-quasiparticle $23/2^{+}$ band in ^{177}Hf are lower than those of the one-quasiparticle bands at the same spin. This is also true when the ratios are plotted against excitation energy [Fig. 9(b)] which suggests that the difference is not due to a trivial effect of the Al front-foils in absorbing lower energy α particles that might plausibly be associated with the population of higher excitation energy states. The lower ratios suggest that the $23/2^{+}$ band receives a higher fractional population from complete fusion when compared to the one-quasiparticle bands.

(iii) The ratios for the five-quasiparticle $39/2^{+}$ band in ^{177}Hf are markedly lower than those for the one-quasiparticle bands; the ratios are also lower than those for the three-quasiparticle $23/2^{+}$ band, until at $I\simeq 18\hbar$, they coincide. This is probably associated with dominance of population via complete fusion at the highest spins, and suggests that $18\hbar$ corresponds to the point where feeding into ^{177}Hf from incomplete fusion drops dramatically. Inspection of Fig. 8 also suggests that the five-quasiparticle states in ^{177}Hf and their associated rotational bands are mainly populated via complete fusion.

(iv) The ratios for the gsb of ^{176}Hf show no dependence on spin. This is consistent with population via complete fusion only, irrespective of whether the α particles are detected in the forward or middle/backward directions. Hence, division of the two feeding patterns that have the same slope produces ratios that show no dependence on spin. If this is indeed the correct explanation, then these ratios should equal unity, which offers the possibility of an approximate empiri-

cal efficiency correction. This suggests that all the ratios should be divided by ~ 2.5

As a final observation, the localized entry-spin distribution of the incomplete fusion process may also explain the population of the less-favored multiquasiparticle states, since none of them (or their associated bands) are fed by the decay of the favored configurations. Most of these states probably lie in the spin region of $\sim 12-15\hbar$, which is consistent with the entry distribution for γ decay following incomplete fusion, as inferred from the F/(M-B) ratios for the gsb in ^{178}Hf shown in Fig. 8.

VI. SUMMARY

In conclusion, high-spin states have been studied in the stable nucleus, ^{177}Hf with the reaction $^{176}\mathrm{Yb}(^{9}\mathrm{Be}, \alpha 4n)^{177}\mathrm{Hf}$. Time-correlated particle-γ-γ coincidence data were collected from which an extensive level scheme has been constructed. Rotational bands based on previously known one- and three-quasiparticle states have been extended to considerably higher spins. A number of new bands were found, and assigned to multiquasiparticle states in ^{177}Hf. One of these was assigned to the previously known $K^{\pi}=19/2^{-}$ three-quasiparticle state which has $T_{1/2}=56$ μs. Two others were assigned to five-quasiparticle states, one of which was the well-known $K^{\pi}=37/2^{-}$ $T_{1/2}$ isomer. The other five-quasiparticle band was assigned to a new $K^{\pi}=39/2^{+}$ state. The g_K values derived from branching ratios were consistent with the assigned configurations in these two and all other cases. Multiquasiparticle calculations were able to reproduce the excitation energies of the observed three- and five-quasiparticle states to within ~ 100 keV. The calculations suggest that all of the most favored three- and five-quasiparticle states were observed.

There is evidence that the states in ^{177}Hf receive population from two distinct entry-spin distributions, one associated with complete fusion of the beam with the target, the other with incomplete fusion that results from beam breakup in the entrance channel. The α-particle yields that are associated with the two distributions are essentially isotropic and forward-peaked, respectively. Ratios of γ-ray intensities in coincidence with α particles detected at forward and middle/backward angles suggest that the highest spin states in ^{177}Hf receive a larger fractional population from complete fusion when compared to states of lower spin.

ACKNOWLEDGMENTS

We would like to thank the academic and technical staff of the ANU Heavy Ion Facility for their support. W. A. S. thanks both the Australian National University and FAPESP (São Paulo) for financial support.

[1] L. Kristensen, M. Jørgensen, O. B. Nielsen, and G. Sidenius, Phys. Lett. **8**, 57 (1964).
[2] P. Alexander, F. Boehm, and E. Kankeleit, Phys. Rev. **133**, B284 (1964).
[3] T. E. Ward and P. E. Haustein, Phys. Rev. Lett. **27**, 685 (1971).
[4] S. M. Mullins, G. D. Dracoulis, A. P. Byrne, T. R. McGoram, S. Bayer, W. A. Seale, and F. G. Kondev, Phys. Lett. B **393**, 279 (1997).
[5] G. D. Dracoulis and A. P. Byrne, Department of Nuclear Physics, Annual Report ANU-P/1052 (1989), p. 115 (unpublished).
[6] G. J. Lane, A. P. Byrne, and G. D. Dracoulis, Department of Nuclear Physics, Annual Report ANU-P/1118 (1992) p. 114 (unpublished).
[7] T. Inamura, M. Ishihara, T. Fukuda, T. Shimoda, and H. Hiruta, Phys. Lett. **68B**, 51 (1977).
[8] D. R. Zolnowski, H. Yamada, S. E. Cala, A. C. Kahler, and T. T. Sugihara, Phys. Rev. Lett. **41**, 92 (1978).
[9] J. Wilczyński, K. Siwek-Wilczyńska, J. Van Driel, S. Gonggrijp, D. C. J. M. Hageman, R. V. F. Janssens, J. Likasiak, R. H. Siemssen, and S. Y. Van Der Werf, Nucl. Phys. **A373**, 109 (1982).
[10] D. C. Radford, Nucl. Instrum. Methods Phys. Res. A **306**, 297 (1995).
[11] G. D. Dracoulis, A. P. Byrne, T. Kibédi, T. R. McGoram, and S. M. Mullins, J. Phys. G **23**, 1191 (1997).
[12] S. Hultberg, I. Rezanka, and H. Ryde, Nucl. Phys. **A205**, 321 (1973).
[13] I. Alfter, E. Bodenstedt, W. Knichel, J. Schüth, and R. Vianden, Z. Phys. A **355**, 363 (1996).
[14] Y. Tanaka, R. M. Steffen, E. B. Shera, W. Reuter, M. V. Hoehn, and J. D. Zumbro, Phys. Rev. C **30**, 350 (1984).
[15] P. M. Walker, G. D. Dracoulis, A. P. Byrne, B. Fabricius, T. Kibédi, A. E. Stuchbery, and N. Rowley, Nucl. Phys. **A568**, 397 (1993).
[16] F. A. Rickey, Jr. and R. K. Sheline, Phys. Rev. **170**, 1157 (1968).
[17] H. I. West, Jr., L. G. Mann, and R. J. Nagle, Phys. Rev. **124**, 527 (1961).
[18] B. D. Jeltema and F. M. Bernthal, Phys. Rev. C **10**, 778 (1974).
[19] I. H. Redmount, T. L. Khoo, and R. A. Warner, Annual Report 1974-75, Michigan State University Cyclotron Laboratory (1975), p. 66.
[20] F. M. Bernthal and J. O. Rasmussen, Nucl. Phys. **A101**, 513 (1967).
[21] Y. Y. Chu, P. E. Haustein, and T. E. Ward, Phys. Rev. C **66**, 2259 (1972).
[22] G. D. Dracoulis, Proceedings of the Conference on Nuclear Structure at the Limits, 1996, Argonne National Laboratory, ANL/PHY-97/1 (1997), p. 148.
[23] G. D. Dracoulis, F. G. Kondev, and P. M. Walker, Phys. Lett. B **419**, 7 (1998).
[24] S. M. Mullins, G. D. Dracoulis, A. P. Byrne, R. A. Bark, S. Bayer, F. G. Kondev, T. R. McGoram, R. T. Newman, and W. A. Seale (unpublished).
[25] F. G. Kondev, G. D. Dracoulis, A. P. Byrne, T. Kibédi, and S. Bayer, Nucl. Phys. **A617**, 91 (1997).
[26] Kiran Jain, P. M. Walker, and N. Rowley, Phys. Lett. B **322**, 27 (1994).